Journal of Vibration Engineering & Technologies (2023) 11:2779–2791
https://doi.org/10.1007/s42417-023-00909-5

ORIGINAL PAPER

Structural Intensity of Laminated Composite Plates Subjected to Distributed Force Excitation

Chendi Zhu[1,2] · **Gang Li**[1,2] · **Shilun Ruan**[1,2] · **Jian Yang**[3,4]

Received: 29 September 2022 / Revised: 14 February 2023 / Accepted: 15 February 2023 / Published online: 3 March 2023

Abstract

Purpose The vibration energy transmission characteristics of laminated composite plates with straight or variable angle fiber paths subjected to distributed force excitations are explored in this paper.

Methods The dynamic responses as a function of frequency are calculated and evaluated using proposed analytical approach and numerical finite element (FE) method based on the first-order shear deformation theory. The FE model is firstly verified by the analytical method and used for the composite plates with various fiber paths. The FE-based structural intensities analysis is carried out to predict the energy transmission and distribution patterns on the laminated composite plates with various fiber paths.

Results The structural intensity streamlines and vectors representation explicitly offer the information of the energy sources, energy sinks and detailed vibration energy distribution and transmission paths. The fiber paths have significant influences on the dynamic responses and energy transmission paths. The results reveal that tailoring fiber paths could lead to the formation of vortex-type flows with low vibration levels.

Conclusion According to the structural intensity fields at the specific excitation frequencies, the tailorable fibers in the forced area or unforced area and curvilinear fibers could be tuned for vibration mitigation.

Keywords Structural intensity · Dynamic response · Laminated composite plates · Vibration energy flow · Energy transmission

Introduction

Composite materials are extensively used in many advanced engineering structures due to their advantageous properties, such as lightweight, high ratios of strength/stiffness-to-weight, good durability, and flexibility in design [1]. Plates are common structural configurations, widely used in aircraft, ships and automobiles. Such structures are usually exposed to complex external dynamic loading and can easily undergo large amplitude vibrations when the excitation frequencies are close to the resonance frequencies. High-level vibrations could result in structural damage, fatigue failure, destruction of engineering systems, and high-level noise pollution. Thus, the knowledge of their dynamic behavior as well as vibration energy transmission mechanisms becomes of high significance in solving vibration problems.

There have been numerous studies devoted to free vibration analysis of laminated composite plates [2]. Several prominent theories have been developed, such as a simplified first-order [3], third-order [4], high-order shear deformation

✉ Gang Li
ligang@dlut.edu.cn

✉ Jian Yang
jian.yang@nottingham.edu.cn

1 Ningbo Institute of Dalian University of Technology, 26 Yucai Road, Ningbo 315016, People's Republic of China

2 State Key Laboratory of Structural Analysis for Industrial Equipment, Department of Engineering Mechanics, Dalian University of Technology, Dalian 116023, People's Republic of China

3 Department of Mechanical, Materials and Manufacturing Engineering, University of Nottingham Ningbo China, 199 Taikang East Road, Ningbo 315100, People's Republic of China

4 International Academy of Marine Economy and Technology (IAMET), University of Nottingham Ningbo China, 199 Taikang East Road, Ningbo 315100, People's Republic of China

theory [5], and a new higher-order shear deformation theory [6]. Recently, modern processing technologies allow the variable angle tow (VAT) composite plates with curved fibers to be created and mechanical behavior of such structures has been investigated [7]. The free vibration analysis of VAT composite plates with arbitrary curvilinear fiber paths was conducted using finite element method, in which natural frequencies and mode shapes were examined [8–10]. It was found that the fundamental natural frequency was increased with implement of optimized curvilinear fibers [11]. There have been some publications on the forced vibration study of conventional composite plates. Dobyns [12] has proposed an analytical approach for forced vibration analysis of simple orthotropic plates subjected to dynamic loadings, and Carvalho et al. [13] studied extensively the effects of impact loads on vibration behavior based on previous work. The experimental investigation on the low-velocity impact loading on dynamic responses of laminated composite plates was developed [14, 15]. The effects of different fiber angles, such as 0°, 45°, and 90°, on the dynamic response of a fiber/epoxy composite plate were investigated experimentally [16]. Although numerous studies focusing on free and forced vibration behavior of a variety of composite plates have been developed, there is limited research associated with vibration energy transmission behavior of VAT plates subjected to complex external dynamic loads.

One of the most effective and reliable tools to predict the energy distribution and transmission paths is via power flow analysis or structural intensity (SI) analysis. SI provides valuable information including the location of sources and energy transmission paths by using vector patterns, which is beneficial to the improved designs of fiber paths. Noiseux [17] measured the vibrational SI in uniform metallic plates and beams experimentally. Gavric and Pavic [18] presented a numerical computation of SI in beams, plates and shells based on a finite element (FE) method. Li and Lai [19] investigated the surface mobility for a thin plate with viscous dampers using FE-based SI analysis. Xu et al. developed the streamline representation which provides more information for the vibration SI fields of the same plate model [20]. The SI of plate structure with multiple dampers was predicted by the FE approach [21]. Xu et al. computed the SI of stiffened plates [22] and that of plates with a hole [23]. The effects of stiffeners and holes on the energy transmission were investigated, respectively. Liu et al. employed SI approach to study dynamic transient response and transient energy transmission of plate structures subjected to low-velocity impact [24] and investigated SI in the box structure for attenuating the vibration and interior noise level [25]. More recently, the energy flow of rectangular plates with stepped thickness was investigated using the FE-based SI analysis [26]. The SI approach was applied to investigate the vibration energy flow in an elastic metamaterial plate with a temperature rise and effects of thermal load on the SI of the cantilevered plate [27, 28]. The potential application of the SI approach in predicting vibration energy transmission behavior has been extensively developed. The energy flow characteristics of metallic flat plate [29], coupled plate [30], L-shaped plate [31–33], and built-up plates in complex forms [34, 35] have been systematically explored. However, there is much less research concerned with the energy flow in composite structures.

There have been recent attempts to investigate the vibration energy transmission on composite plates. For instance, the SI on composite orthotropic panels was carried out by experimental and numerical methods and compared with that on the aluminum sandwich panels [36]. The influences of damping, loadings, constraints, thickness, and fibers orientations were analyzed. Two different numerical models including solid and shell elements were evaluated for the accuracy of SI in a fiber composite plate [37]. Zhu et al. have studied the vibration energy transmission on square laminated composite plates and the inerter-based passive device was applied for vibration suppression [38]. The power flow analysis of composite plates coupled in L-shape was carried out adopting a substructure method [39, 40]. The energy transmission behavior of composite plates with curvilinear fibers harmonically excited by the point force has been evaluated [41]. The force vibration analysis of composite plates with various fibers excited by the point force has been investigated. However, there has been limited work on distributed force excitation case [42]. In addition, the designs of tailorable fibers for desired vibration performance have received little attention. Hence, they are taken into account subsequently.

This study has emphasized the SI streamlines and vectors representation of laminated composite plates with various fiber paths excited by distributed force. Adopting SI technologies, the forced vibration behavior of a variety of composite plates is detected and evaluated from the energy flow viewpoint. The effects of loading types and various fiber paths on energy transmission patterns are discussed. The energy transmission between the forced and unforced areas is investigated. Furthermore, advantages of VAT plate are yielded by comparison with straight fiber cases. The results are expected to provide useful information on variable stiffness designs for enhanced vibration suppression.

Model Description

Figure 1a illustrates a schematic diagram of a rectangular laminated composite plate of N layers with length of a, width

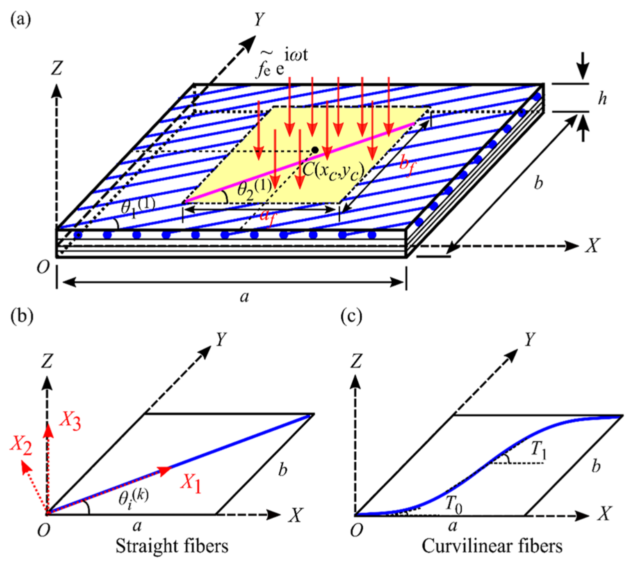

Fig. 1 A schematic illustration of **a** a rectangular laminated composite plate subjected to distributed area force excitation; **b** the *k*th layer of the plate with straight fibers, and **c** with curvilinear fibers

of b, and thickness of h in the OX, OY, and OZ directions, respectively. Distributed harmonic excitation force of $\widetilde{f}_e e^{i\omega t}$ is uniformly distributed over the contact area of side lengths a_f and b_f with the center at the point $C(x_c, y_c)$. The fiber orientations of the unforced area and forced area on the kth layer are denoted by $\theta_1{}^{(k)}$ and $\theta_2{}^{(k)}$, respectively. It is noted that for the laminated composite plate with conventional straight fibers, the value of $\theta_1{}^{(k)}$ is as the same as that of $\theta_2{}^{(k)}$ while different values of $\theta_1{}^{(k)}$ and $\theta_2{}^{(k)}$ lead to a simple lamination scheme for variable stiffness composite plates. In Fig. 1b, this is the kth layer of a lamina with straight fibers, showing the principal material coordinate system of $OX_1X_2X_3$ and the laminate coordinate system of $OXYZ$. Figure 1c shows a layer of curvilinear fibers with the notation of $\langle T_0, T_1 \rangle$, in which T_0 and T_1 are the fiber angles at $x = 0$ and $x = a/2$, respectively. The fiber orientations of curvilinear fiber paths at any point (x, y) are descripted and defined as the function of x in the laminate coordinate system of OXY as:

$$\theta(x) = \frac{2(T_1 - T_0)x}{a} + T_0, \quad \text{when} 0 \le x \le \frac{a}{2}; \tag{1a}$$

$$\theta(x) = \frac{2(T_0 - T_1)\left(x - \frac{a}{2}\right)}{a} + T_1, \quad \text{when} \frac{a}{2} \le x \le a. \tag{1b}$$

Analytical Solutions of Dynamic Responses

The theoretical solution of dynamic responses for several special symmetric orthotropic laminated plates with simple straight fibers in $[0°]_4$ or $[90°]_4$ is available. For those plates, some stress stiffness coefficients, such as A_{16}, A_{26}, B_{ij}, D_{16}, and D_{26}, are zero. As a result, a reduced form of equations of motion for vibration analysis according to FSDT can be expressed as [13]:

$$kS_{44}\left(\frac{\partial^2 w_0}{\partial y^2} + \frac{\partial \phi_y}{\partial y}\right) + kS_{55}\left(\frac{\partial^2 w_0}{\partial x^2} + \frac{\partial \phi_x}{\partial x}\right) + q_z = \rho h \ddot{w}, \tag{2a}$$

$$\begin{aligned} &D_{11}\frac{\partial^2 \phi_x}{\partial x^2} + \left(D_{12} + D_{66}\right)\frac{\partial^2 \phi_y}{\partial xy} + D_{66}\frac{\partial^2 \phi_x}{\partial y^2} \\ &- kS_{55}\left(\frac{\partial w_0}{\partial x} + \phi_x\right) = \frac{\rho h^3}{12}\ddot{\phi}_x, \end{aligned} \tag{2b}$$

$$\begin{aligned} &D_{66}\frac{\partial^2 \phi_y}{\partial x^2} + \left(D_{12} + D_{66}\right)\frac{\partial^2 \phi_x}{\partial xy} + D_{22}\frac{\partial^2 \phi_y}{\partial y^2} \\ &- kS_{44}\left(\frac{\partial w_0}{\partial y} + \phi_y\right) = \frac{\rho h^3}{12}\ddot{\phi}_y, \end{aligned} \tag{2c}$$

where h is the thickness of plate; ρ is the material density; q_z is the applied external load; and k is a shear correction factor in FSDT and is popularly taken to be 5/6 [1]. Terms A_{ij}, B_{ij}, D_{ij} and S_{ij} represent the stiffnesses, which are defined as

$$\left(A_{ij}, B_{ij}, D_{ij}\right) = \int_{-h/2}^{h/2} Q_{ij}\left(1, z, z^2\right)\mathrm{d}z, i, j = 1, 2, 6, \tag{3a}$$

$$S_{ij} = \int_{-h/2}^{h/2} c_{ij}\mathrm{d}z, i, j = 4, 5. \tag{3b}$$

For the simply supported boundary condition, it can be assumed that $w = 0$ and $\partial\phi_x/\partial x = 0$ at $x = 0$ and $x = a$, and $w = 0$ and $\partial\phi_y/\partial y = 0$ at $y = 0$ and $y = b$. Using the Navier's approach, the double Fourier series for the rotations and transverse displacement of a simply supported rectangular plate are given by [13]:

$$\phi_x(x, y, t) = \sum_m \sum_n A_{mn}(t) \cos \alpha x \sin \beta y, \tag{4a}$$

$$\phi_y(x, y, t) = \sum_m \sum_n B_{mn}(t) \sin \alpha x \cos \beta y, \tag{4b}$$

$$w(x, y, t) = \sum_m \sum_n W_{mn}(t) \sin \alpha x \sin \beta y, \tag{4c}$$

where $\alpha = m\pi/a$ and $\beta = n\pi/b$, m and n are integers, and $A_{mn}(t)$, $B_{mn}(t)$, and $W_{mn}(t)$ are time-dependent coefficients. The double Fourier series for external load is written as:

$$q_z(x,y,t)=\sum_m\sum_n Q_{mn}(t)\sin\alpha x\sin\beta y, \tag{5}$$

where $Q_{mn}(t)$ is the term of the Fourier series.

For the point force located at the point (x_p, y_p), the $Q_{mn}(t)$ is expressed as:

$$\begin{aligned}Q_{mn}(t)&=\frac{4}{ab}\int_0^a\int_0^b p(x,y,t)\sin\alpha x\sin\beta y\mathrm{d}x\mathrm{d}y\\&=\frac{4f(t)}{ab}\sin\alpha x_p\sin\beta y_p.\end{aligned} \tag{6}$$

where $p(x,y,t)=f(t)\delta\left(x-x_0,y-y_0\right)$; $\delta(x,y)$ is a two-dimensional Dirac's delta function.

For the uniformly distributed force over the area a_f and b_f with center at (x_c, y_c), we have

$$\begin{aligned}Q_{mn}(t)&=\frac{16}{mn\pi^2}\int_{x_c-\frac{a_f}{2}}^{x_c+\frac{a_f}{2}}\int_{y_c-\frac{b_f}{2}}^{y_c+\frac{b_f}{2}}p(x,y,t)\sin\alpha x\sin\beta y\mathrm{d}x\mathrm{d}y\\&=\frac{16f(t)}{mn\pi^2}\sin\alpha x_c\sin\beta y_c\sin\alpha\frac{a_f}{2}\sin\beta\frac{b_f}{2}.\end{aligned} \tag{7}$$

Substituting Eqs. (4) and (5) into Eq. (2) results in the simplified equation of motion [13]

$$\begin{bmatrix}L_{11}&L_{12}&L_{13}\\L_{12}&L_{22}&L_{23}\\L_{13}&L_{23}&L_{33}\end{bmatrix}\begin{Bmatrix}A_{mn}(t)\\B_{mn}(t)\\W_{mn}(t)\end{Bmatrix}=\begin{Bmatrix}0\\0\\Q_{mn}(t)-\rho h\ddot{W}_{mn}(t)\end{Bmatrix}, \tag{8}$$

in which, L_{ij} are defined as:

$$L_{11}=D_{11}(\alpha)^2+D_{66}(\beta)^2+kA_{55}, L_{12}=\left(D_{12}+D_{66}\right)\alpha\beta,$$

$$L_{13}=kA_{55}\alpha, L_{22}=D_{66}\alpha^2+D_{22}\beta^2+kA_{44},$$

$$L_{23}=kA_{44}\beta, L_{33}=kA_{55}\alpha^2+kA_{44}\beta^2. \tag{9}$$

The terms of $A_{mn}(t)$ and $B_{mn}(t)$ can be rewritten following transformation

$$A_{mn}(t)=\frac{L_{12}L_{23}-L_{13}L_{22}}{L_{11}L_{22}-L^2{}_{12}}W_{mn}(t),$$

$$B_{mn}(t)=\frac{L_{12}L_{13}-L_{11}L_{23}}{L_{11}L_{22}-L^2{}_{12}}W_{mn}(t). \tag{10}$$

As a result, Eq. (8) can be reduced to the following form

$$\ddot{W}_{mn}(t)+\omega^2{}_{mn}W_{mn}(t)=\frac{Q_{mn}(t)}{\rho h}. \tag{11}$$

The natural frequencies for calculation of dynamic responses can be determined by

$$\omega_{mn}=\sqrt{\frac{1}{\rho h}\left(L_{33}+\frac{2L_{12}L_{23}L_{13}-L_{22}L^2{}_{13}-L_{11}L^2{}_{23}}{L_{11}L_{22}-L^2{}_{12}}\right)}. \tag{12}$$

In a damped system, the distributed proportional damping can be taken into account using complex eigenfrequencies. The internal damping of the structure is represented by a modal loss factor η. As a result, the dynamic response at any point (x, y) on the composite plate subjected to the point force can be obtained from

$$w(x,y,t)=\frac{4\tilde{f}_{\mathrm{e}}}{ab\rho h}\sum_m\sum_n\frac{\sin\alpha x_p\sin\beta y_p\sin\alpha x\sin\beta y}{\omega^2{}_{mn}(1+\mathrm{i}\eta)-\omega^2}\mathrm{e}^{\mathrm{i}\omega t}, \tag{13}$$

and that of the plate subjected to the area force excitation is expressed as

$$w(x,y,t)=\frac{16\tilde{f}_{\mathrm{e}}}{\pi^2 mn\rho h}\sum_m\sum_n\frac{\sin\alpha x_c\sin\beta y_c\sin\alpha\frac{a_f}{2}\sin\beta\frac{b_f}{2}\sin\alpha x\sin\beta y}{\omega^2{}_{mn}(1+\mathrm{i}\eta)-\omega^2}\mathrm{e}^{\mathrm{i}\omega t}. \tag{14}$$

Structural Intensity Analysis

Structural intensity (SI) is a vector field in a continuum as defined in Ref. [18]. The instantaneous SI component in the time domain can be expressed by dot product of velocity vector v_j and stress tensor σ_{jk}:

$$I_i=\langle I_i(t)\rangle=\langle-\sigma_{ij}(t)v_j(t)\rangle, i,j=1,2,3, \tag{15}$$

where $\sigma_{ij}(t)$ and $v_j(t)$ are the stress and velocity in the jth-direction at time t.

For the steady-state vibration, the ith-direction of SI in a frequency domain is given by

$$I_i(\omega)=-\frac{1}{2}\Re\left(\tilde{\sigma}_{ij}(\omega)\tilde{v}_j^*(\omega)\right), i,j=1,2,3. \tag{16}$$

Hence, with a time-averaged quantity, the two components of the SI combining shear, bending, twisting waves as shown in Fig. 2 for a vibrating plate are given by [18, 43]

$$I_x=-\frac{1}{2}\Re\left\{Q_x\tilde{\dot{w}}_z^*+N_{xy}\tilde{\dot{w}}_y^*+N_{xx}\tilde{\dot{w}}_x^*-M_{xy}\tilde{\dot{\theta}}_x^*-M_{xx}\tilde{\dot{\theta}}_y^*\right\}, \tag{17}$$

$$I_y=-\frac{1}{2}\Re\left\{Q_y\tilde{\dot{w}}_z^*+N_{xy}\tilde{\dot{w}}_x^*+N_{yy}\tilde{\dot{w}}_y^*-M_{xy}\tilde{\dot{\theta}}_y^*-M_{yy}\tilde{\dot{\theta}}_x^*\right\}, \tag{18}$$

where N_{xx}, N_{yy} and N_{xy} are complex membrane forces; M_{xx}, M_{yy} and M_{xy} are complex internal moments; Q_x and Q_y are complex transverse shear forces; $\tilde{\dot{w}}_x^*, \tilde{\dot{w}}_y^*, \tilde{\dot{w}}_z^*$ are complex

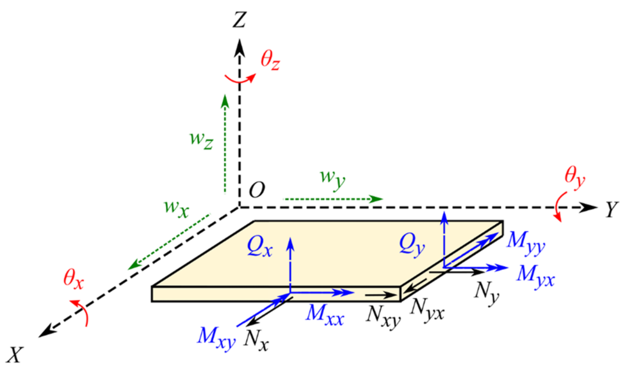

Fig. 2 Forces and displacements in a plate element

conjugate displacements in the directions of OX, OY and OZ directions, respectively; and $\tilde{\dot{\theta}}_x^*$, $\tilde{\dot{\theta}}_y^*$ are complex conjugate rotations about the directions of OX and OY, respectively.

The structural intensity streamline can be expressed as

$$\mathrm{d}\mathbf{r} \times \mathbf{I}(\mathbf{r}, t) = 0, \tag{19}$$

where $\mathbf{r}$ represents the position of energy flow particle. The SI of an energy flow element on such a streamline is perpendicular to $\mathbf{r}$ and is parallel to $\mathrm{d}\mathbf{r}$ [24]. For the steady-state energy flows, the cross product can be expressed as

$$\begin{vmatrix} \mathbf{i} & \mathbf{j} & \mathbf{k} \\ I_x & I_y & I_z \\ \mathrm{d}x & \mathrm{d}y & \mathrm{d}z \end{vmatrix} = 0. \tag{20}$$

As a result, the equation describing SI streamline in a two-dimensional plate structure is

$$\frac{\mathrm{d}x}{I_x} = \frac{\mathrm{d}y}{I_y}. \tag{21}$$

Results and Discussion

The proposed analytical and FE numerical method based on FSDT are used to investigate the vibration characteristics of various laminated composite plates. This plate with simply supported edges is constructed from four plies of T300/934 CFRP material with structural damping of $\eta = 0.01$. The fiber angles of all layers are the same. The material properties of the plate are as follows: $E_1 = 120\text{GPa}$, $E_2 = 7.9\text{Gpa}$, $G_{12} = 5.5\text{Gpa}$, $G_{23} = 1.58\text{Gpa}$, $v_{12} = 0.33$, $\rho = 1580\text{kg/m}^3$.

The proposed analytical solution for special cases of simple orthotropic laminates plate with 0° or 90° straight fibers is available and is used to validate the FE model. In the analytical solution, m and n of 100 are selected with a balanced consideration of the computation cost and accuracy.

For the composite plate with various fiber paths, a numerical FE-based method based on ANSYS is employed. In ANSYS, the four-node Shell-181 element is used for building a plate model, which is suitable for thin to moderately thick shell structure. The plate is divided into 800 elements with mesh size of 0.025 m and 0.025 m. There are 5 independent degrees of freedom and 1 dependent one for each node for the Shell 181 element. The accuracy in FE modeling is governed by the FSDT. Three integration points are used through the thickness, in which two points are located on the top and bottom surfaces, and the remaining point is at the midway between those two points.

Vibration Energy Transmission on Laminated Composite Plates

A parametric study on the forced vibration behavior of laminated composite plates subjected to various loadings is carried out. This analytical method is used to validate the numerical FE method. Figure 3 shows the displacement amplitude W_A at the point A as a function of non-dimensionalized frequency $\left(\overline{\varpi} = \omega(a^2/h)\sqrt{\rho/E2}\right)$ of the $[0°]_4$ laminated composite plate at its center point. In the first case as Fig. 3a has shown, laminated composite plates with different dimensions are subjected to the point force at the center point. It is found that much more modes are excited by the applied force when the ratio of a/b is 0.5 and with the increases of ratios of a/b, the numbers of resonance peaks decreased. The amplitudes of the response of the first peak are increased when the value of the a is larger than b for the composite plate of $[0°]_4$. In Fig. 3b, dynamic responses of the square composite plate with $a_f = 0.5a = 0.5b$ subjected to the area force with different ratios of a_f/b_f are investigated. The ratios of 0.5, 1, and 2 are considered. Increasing ratios of a_f/b_f lead to the reduction of dimension of distributed area force. It is found that amplitudes of the resonance peaks are reduced by increasing the ratios of a_f/b_f. Figure 3c shows the effects of the relation between the area of the load excitation force and the area of plate (i.e., the value of a_f/a) on dynamic response of the rectangular composite plate ($a/b = 2$) with distributed area force of $a_f/b_f = 2$. The values of a_f/a vary from 0.25, to 0.5, and to 0.75. It is found that the response amplitude of the first peak increases with the value of a_f/a as the area of applied force extended.

In this study, a rectangular composite plate with the structural dimensions with $a = 1$ m, $b = 0.5$ m and the thickness of $t = 0.005$ m is considered for demonstration of the proposed analysis approach on effects of fiber orientations. Other values for the dimensions of the plate could also be used following the same analysis procedure and

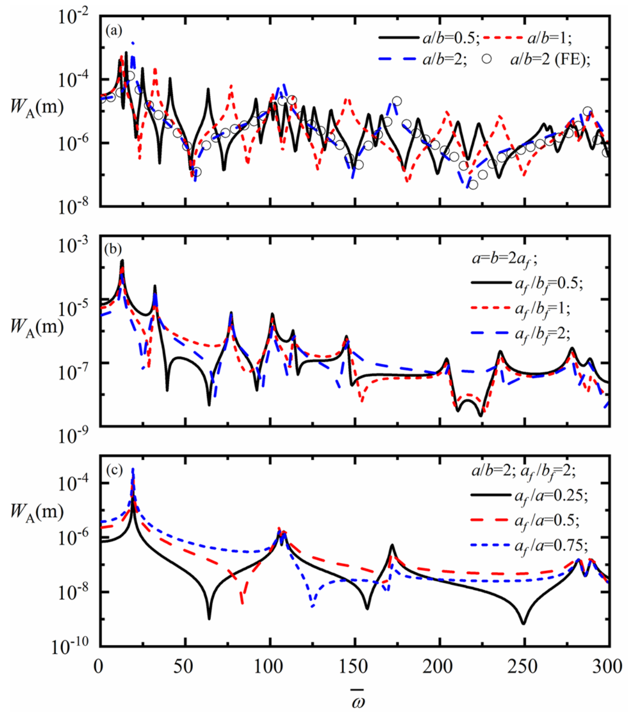

Fig. 3 The amplitude of the response (W_A) as a function of the non-dimensionalized frequency ($\overline{\omega} = \omega(a^2/h)\sqrt{\rho/E2}$) at the center point on the laminated composite plate in $[0°]_4$ with various excitations. **a** Plates with different dimensions subjected to the point force; **b** plates subjected to the area force with different ratios of a_f/b_f; **c** plates subjected to the area force with different ratios of a_f/a. Circles represent corresponding numerical results

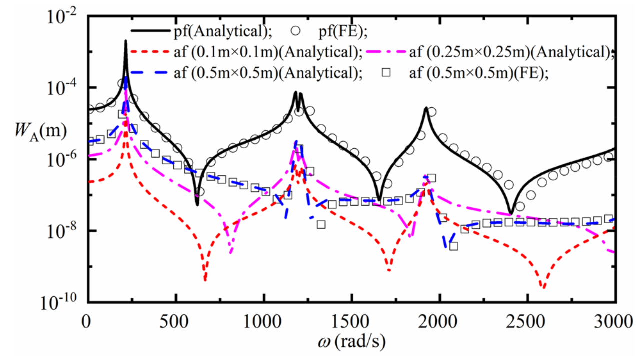

Fig. 4 The amplitude of the response (W_A) as a function of the frequency at the center point (0.5 m, 0.25 m) on the rectangular laminated composite plate in $[0°]_4$ with various excitations. Solid line: the point force (i.e., pf); dashed line: the area force (i.e., af) over the area of 0.1 m and 0.1 m; dash-dotted line: the area force over the area of 0.25 m and 0.25 m; and dashed space line: the area force over the area of 0.5 m and 0.5 m. Circles and squares represent corresponding numerical results

the established model. Figure 4 shows the displacement amplitude W_A of the point (0.5 m, 0.25 m) as a function of frequency of the $[0°]_4$ laminated composite plate in an examined frequency range of 0–3000 rad/s. Several types of excitation loads, such as a point force and distributed area force, with amplitude of 1 N are applied at such plate. Four cases (i.e., cases 1–4) such as the point force, the distributed force over the contact area of 0.1 m × 0.1 m, 0.25 m × 0.25 m, and 0.5 m × 0.5 m, are selected for comparison. The corresponding results of cases 1–4 based on the proposed analytical method are denoted by solid, dotted, dash-dotted, and dashed lines, respectively. The circles and squares are for numerical FE results for validation. In cases 1 and 4, a great agreement between analytical and numerical results is found and therefore, the proposed analytical methods for determination of the response of composite plates excited by the point force or area force are verified, respectively. It is found that the plate is easily excited by the applied force approximately at $\omega = 213.63$ rad/s. The peak value of each resonance peak of the plates excited by point force is higher than that by area force. A comparison of cases 2–4 shows that the amplitudes of the first peak decrease with the reduction of contacted area. The peaks of these four cases are close but their valleys are varied. With the increase of excitation frequencies, it is found that the amplitudes of the response of the plate subjected to area force excitation are generally lower than that with the point force. This analytical method could be applied to predict the response as a function of frequency at any point of conventional composite plates efficiently with relatively low computational costs than full FE methods.

Figure 5 shows the amplitude of the response as a function of frequency of laminated composite plates subjected to the area force excitation with variations of the fiber orientations. The contact area is set as 0.25 m and 0.25 m. Such dimension of the area force is proper to clearly observe the energy transmission paths especially between the forced and unforced areas. The fiber orientations, such as $[0°]_4$, $[30°]_4$, $[45°]_4$, $[60°]_4$, and $[90°]_4$, are selected for investigation, labeled as cases 1–5, respectively. In this case, the numerical FE methods are mainly utilized. It is found that the increase of fiber orientations from 0° to 90° leads to the increase of the first resonance frequency from 213.63 to 508.94 rad/s and reduction of peak values of first resonance peak. In contrast, the resonance frequencies of their second peaks increase with the decrease of fiber angles. As a result, it is seen that the frequency range from the first peak to second peaks is narrowed as the fiber angle increased. This of the case 5 (i.e., 90°) is the narrowest. The first peak value of case 1 can be reduced by increasing the fiber angle. In a prescribed excitation frequency range from 1350 to 1750 rad/s, tailoring the fiber angle in 30° effectively lowers the amplitude of the response as a function of frequency and suppress the vibration. As the excitation frequency increased, the dynamic responses for each case generally become relatively lower.

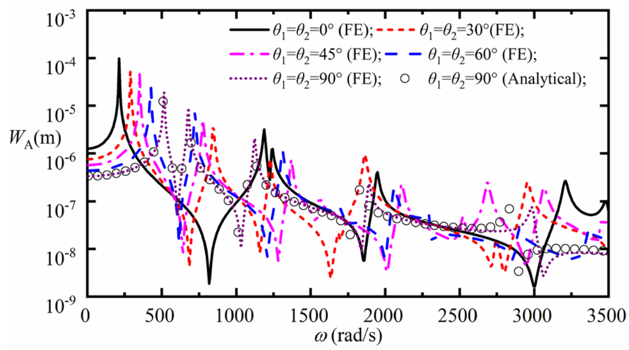

Fig. 5 The amplitude of the response (W_A) as a function of the frequency at the center point (0.5 m, 0.25 m) on the rectangular laminated composite plates with various fiber angles subjected to the distributed force over the area of 0.25 m and 0.25 m. Solid line: the $[90°]_4$ plate; short dashed line: the $[30°]_4$ plate; dash-dotted line: the $[45°]_4$ plate; dashed space line: the $[60°]_4$ plate; and dotted line: the $[90°]_4$ plate. Circles represent corresponding analytical results

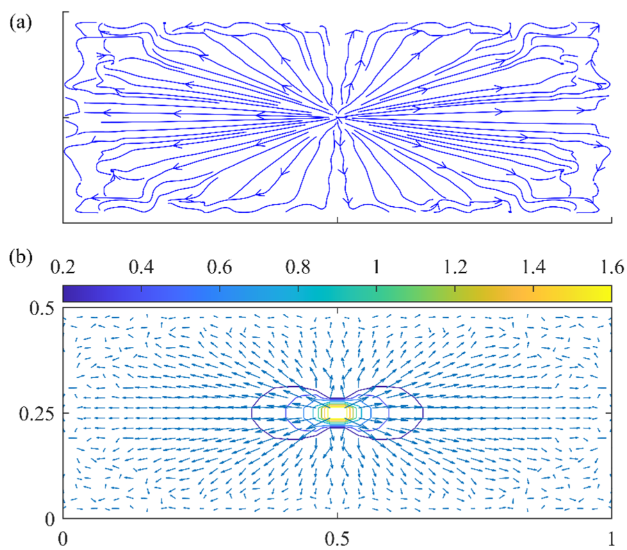

Fig. 6 Structural intensity in the laminated composite plate with $\theta_1 = \theta_2 = 0°$ with point force excitation at the center point (0.5 m, 0.25 m) at a frequency of 213.63 rad/s. **a** Streamline and **b** vector

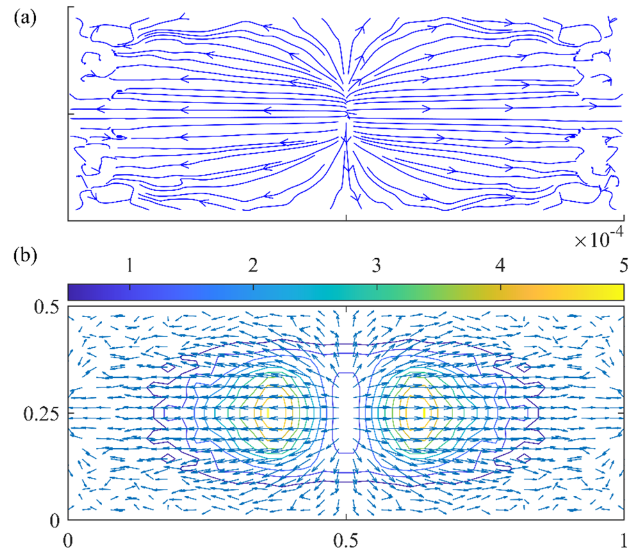

Fig. 7 Structural intensity in the laminated composite plate with $\theta_1 = \theta_2 = 0°$ with area force excitation over the area of 0.25 m and 0.25 m at the center point (0.5 m, 0.25 m) at a frequency of 213.63 rad/s. **a** Streamline and **b** vector

Figures 6 and 7 show the SI fields on the $[0°]_4$ composite plate subjected to the point force and the distributed force with contact area of 0.25 m and 0.25 m at the center point (0.5 m, 0.25 m), respectively. The SI was performed at the first excitation frequency of 213.63 rad/s and SI fields are illustrated by streamlines and vectors, respectively. The location of source and energy transmission paths are identified both by streamlines and vectors representations. In Fig. 5, the energy source is generated at the forcing position. Due to effects of the point force, an energy source is generated at the center point and most of energy flows to the left and right edges, following the fiber orientations in 0°. As a result, serried streamlines in the horizontal direction are found in Fig. 6a. Figure 6b shows that some vectors from the energy source are pointing at the horizontal direction and there is no obvious energy sink formed. From the streamlines plots in Fig. 7a, it is found that the number of the horizontal streamlines increases when the area force is applied. As Fig. 7b has shown, the area of energy source is extended with the applied area force, and the vectors with relatively large magnitudes are distributed around the energy source. The magnitudes of SI vectors on the plate subjected to the area force are much lower than that of the plate subjected to point force. It is observed that the streamline visualization technique is able to clearly depict the energy flow paths in the regions of relatively small magnitude than vectors, but vectors effectively indicate the relative magnitudes of structural intensities.

Here the effects of fiber angles on the SI of the $[45°]_4$ and $[90°]_4$ laminated composite plates are investigated in Figs. 8 and 9. They are for the cases 3 and 5 examined in Fig. 4, excited at 772.83 rad/s and 672.30 rad/s, respectively. Figure 8a clearly shows the structural intensity streamline under the area force excitation. It is found that the streamlines in the vicinity of center point are distorted by the fiber angles larger than 0°. The streamline representation explicitly shows the energy transmission paths, in which the majority of energy flows into the left-top and right-bottom part of the plate. The position of energy source is the center part of the plate as shown in Fig. 8a. Most of vectors are aligned

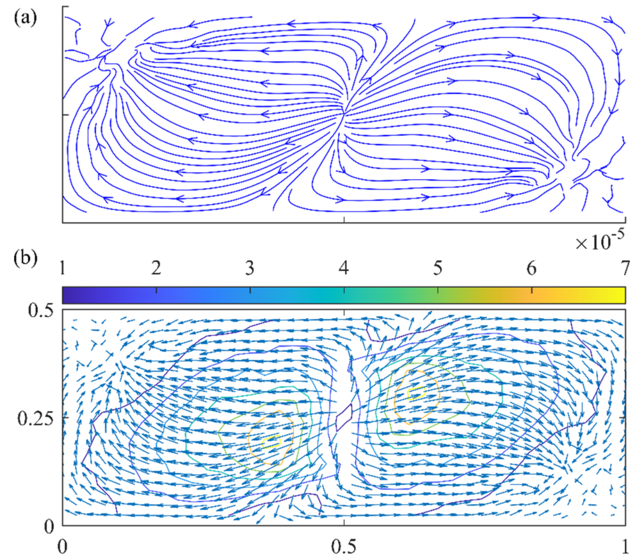

Fig. 8 Structural intensity in the laminated composite plate with $\theta_1 = \theta_2 = 45°$ with area force excitation over the area of 0.25 m and 0.25 m at center point (0.5 m, 0.25 m) at a frequency of 772.83 rad/s. **a** Streamline and **b** vector

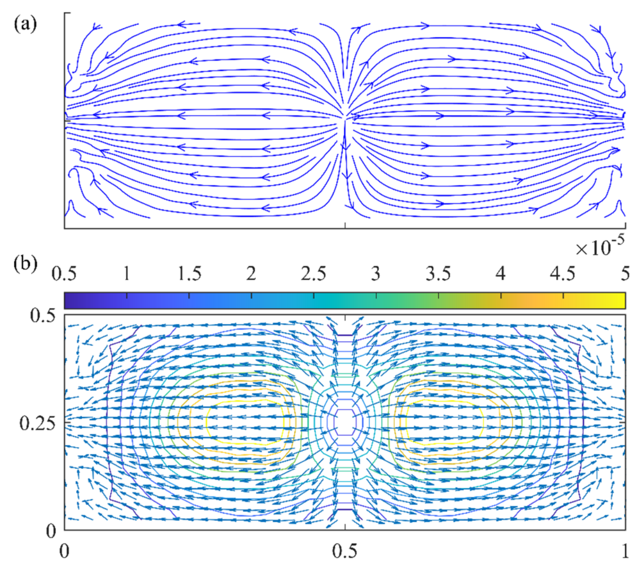

Fig. 9 Structural intensity in the laminated composite plate with $\theta_1 = \theta_2 = 90°$ with area force excitation over the area of 0.25 m and 0.25 m at center point (0.5 m, 0.25 m) at a frequency of 672.30 rad/s. **a** Streamline and **b** vector

with the fiber angles in 45°, and the contours with high magnitudes are distributed around the center part, along the direction of fiber angles. When the fiber angle is increased from 45° to 90°, streamlines at the middle line are rotated with the direction of anti-clockwise as shown in Fig. 9a. The energy transmission paths become symmetric about the middle line. In Fig. 9b, the number of the vectors pointing at the horizontal direction is increased while most energy flows into the middle point of the left and right edges of the plate. A comparison between those two cases shows that the positions of energy sink are changed from left-top and right-bottom part to middle point of the left and right edges by altering the fiber orientations from 45° to 90°.

Effects of Fiber Orientation of the Forced Area

The foregoing investigation indicates that the fiber orientation could be designed to suppress the vibration level. In this section, the influences of tailorable fiber paths in the forced area on the response amplitude as a function of frequency and structural intensities of variable stiffness plate are investigated. The area force excitation is applied at the center point (0.5 m, 0.25 m) with contact area of 0.25 m and 0.25 m. Five cases are compared as the fiber angles of the unforced area are fixed as $\theta_1 = 0°$, while that of the forced area is set at $\theta_2 = 0°$, 30°, 45°, 60°, and 90° for cases 1–5, respectively. Figure 9 shows the variations of the amplitude of the response as a function of the excitation frequency of laminated composite plates with different fiber angles in the forced area. The corresponding results are represented by solid, short dashed, dash-doted, dashed, and dotted lines, respectively. It is found that their first peaks are close with varied peak values. By increasing the fiber angle of θ_2, the first peak values are reduced to some extent. The vibration level is reduced by increasing the fiber angle in the forced area that increases the stiffness in lateral direction. It is seen that the effects of peak values of θ_2 on the second peaks values are significantly larger than first peak. The second resonance frequencies of cases 2–5 are lower than that of case 1 (i.e., $\theta_1 = \theta_2 = 0°$). The peak values of the second peaks of cases 2–4 are much lower than the first one. The comparison between five cases indicates that the dynamic responses of the $[0°]_4$ laminated composite plate in the excitation frequency of 1000–1500 rad/s could be effectively reduced by tailoring the fiber angles in the forced area (Fig. 10).

Figures 11 and 12 demonstrate the streamlines and vectors of structural intensities on the aforementioned specific laminated composite plate with $\theta_2 = 30°$ and $\theta_2 = 60°$. They are excited by the distributed force at the frequency of 873.36 rad/s and 879.65 rad/s. Figure 11a shows that the directions of streamlines within the forced area are related to the designed fiber angle in 30°. There are two recirculation regions formed on the top and bottom of the center part. The streamlines around recirculation regions become serried. In Fig. 11b, large amount of energy from the source is flowing in a clockwise direction due to the effects of vortex-type flow. As a result, there is no energy sink formed on the plate. In contrast, when the fiber angle is increased from 30° to 60°, the positions of two recirculation regions are shifted to center part of the plate as shown in Fig. 12a. A vortex-type

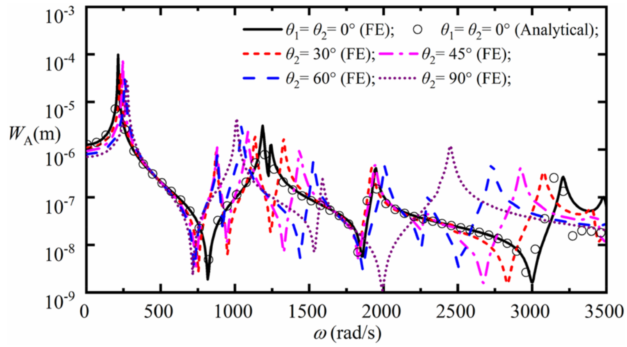

Fig. 10 The amplitude of the response (W_A) as a function of frequency at the center point (0.5 m, 0.25 m) on the laminated composite plate with $\theta_1 = 0°$ subjected to the area force over the area of 0.25 m and 0.25 m. Solid line: $\theta_2 = 0°$; short dashed line: $\theta_2 = 30°$; dash-dotted line: $\theta_2 = 45°$; dashed space line: $\theta_2 = 60°$; and dotted line: $\theta_2 = 90°$. Circles represent corresponding analytical results

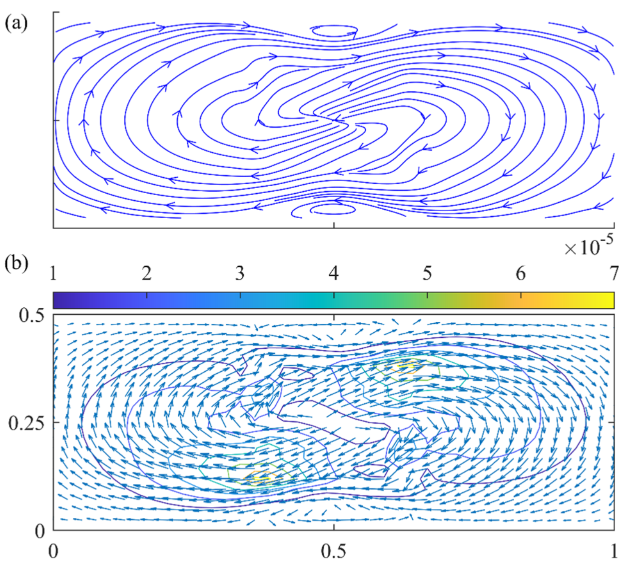

Fig. 11 Structural intensity in the laminated composite plate with $\theta_1 = 0°$ and $\theta_2 = 30°$ with area force excitation over the area of 0.25 m and 0.25 m at center point (0.5 m, 0.25 m) at a frequency of 873.36 rad/s. **a** Streamline and **b** vector

flow generally following a clockwise direction is observed. In Figs. 11b and 12b, the vectors with relative high magnitudes are distributed around the interface between the forced and unforced areas. Comparing Figs. 11 and 12 with 8–9, it is found that the contours with high magnitudes in these two cases are relatively small than that in Figs. 8 and 9. At such particular excitation frequencies, the low vibration levels of laminated composite plates are likely contributed by the formation of vortex-type flow.

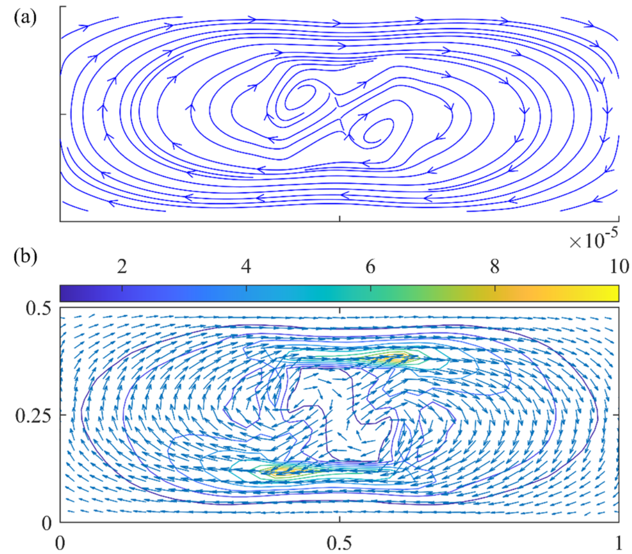

Fig. 12 Structural intensity in the laminated composite plate with $\theta_1 = 0°$ and $\theta_2 = 60°$ with area force excitation over the area of 0.25 m and 0.25 m at center point (0.5 m, 0.25 m) at a frequency of 879.65 rad/s. **a** Streamline and **b** vector

Effects of Fiber Orientation of the Unforced Area

The influences of tailorable fiber orientation at the unforced area on the response amplitude and structural intensities of variable stiffness plates are investigated regarding to the case where the structural parameters of the contacted area are fixed. The fiber angle of forced area is set as $\theta_2 = 90°$ and that of unforced area could be designed as $\theta_1 = 90°$, 60°, 45°, 30°, and 0° for cases 1–5, respectively. Figure 13 shows the variations of the response amplitude at the point (0.5 m, 0.25 m) with different fiber paths. The corresponding results are denoted by solid, short dashed, dash-doted, dashed, and

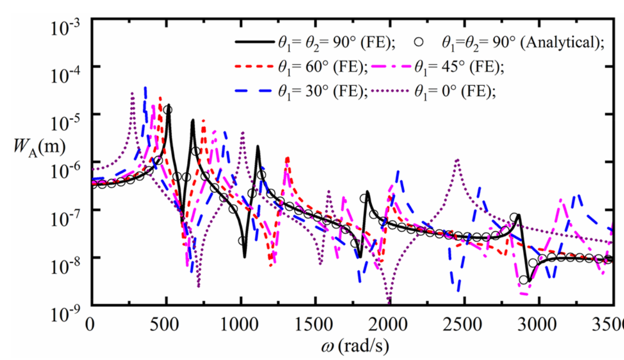

Fig. 13 The amplitude of the response (W_A) as a function of frequency at the center point (0.5 m, 0.25 m) on the laminated composite plate with $\theta_2 = 90°$ subjected to the area force over the area of 0.25 m and 0.25 m. Sold line: $\theta_1 = 90°$; short dashed line: $\theta_1 = 60°$; dash-dotted line: the $\theta_1 = 45°$; dashed space line: $\theta_1 = 30°$; and dotted line: $\theta_1 = 0°$. Circles represent corresponding analytical results

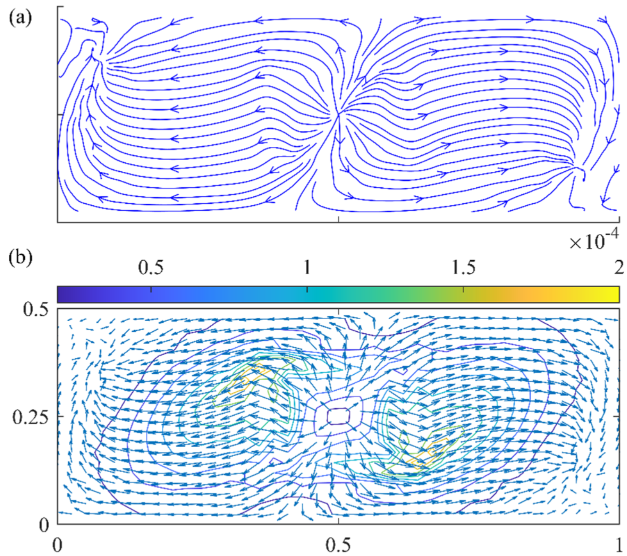

Fig. 14 Structural intensity in the laminated composite plate with $\theta_1 = 60°$ and $\theta_2 = 90°$ with area force excitation over the area of 0.25 m and 0.25 m at center point (0.5 m, 0.25 m) at a frequency of 747.70 rad/s. **a** Streamline and **b** vector

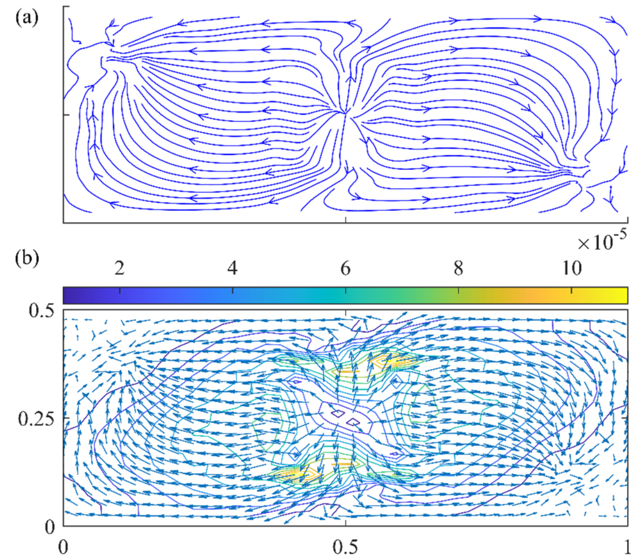

Fig. 15 Structural intensity in the laminated composite plate with $\theta_1 = 30°$ and $\theta_2 = 90°$ with area force excitation over the area of 0.25 m and 0.25 m at center point (0.5 m, 0.25 m) at a frequency of 892.21 rad/s. **a** Streamline and **b** vector

dotted lines, respectively. For case 1, a fine mesh size of 0.0125 m is used in FE model. A comparison of solid line and circles shows that numerical results especially in high-frequency ranges have good agreement with that of analytical method and the convergence is achieved. It is found that the first resonance frequencies increase with the fiber angle of θ_2 but amplitudes of the first peaks are varied. The peak value of case 3 (i.e., $\theta_1 = 45°, \theta_2 = 90°$) is found to be the lowest. In contrast, decrease in the fiber angle of θ_1 leads to the increase of second resonance frequencies; the peak value of second peak of case 3 is also the lowest. This yields the finding that the frequency range between the first and second peaks could be effectively shortened by increasing the fiber angles of uncontacted area.

The influences of the fiber angles of uncontacted area on the vibration energy transmission patterns are of interest. Figures 14, 15, and 16 present SI streamlines and vectors on the laminated composite plates for $\theta_2 = 90°$ and $\theta_1 = 60°$, 30°, and 0°, excited at 747.70 rad/s, 892.21 rad/s, and 1005.31 rad/s, respectively. For comparison, Fig. 9 showing the SI of the plate for the case 1 with $\theta_1 = \theta_2 = 90°$ excited at 672.30 rad/s is recalled. Compared to SI in Fig. 9, the streamline in the Fig. 14a is found to be that less energy is pointing at the fiber angle in 90° and most of that is altered due to the effects of the 60° fiber angle at uncontacted area. The energy finally flows into left-top and right-bottom part of the plate along the 60° fiber angle. In Fig. 14b, it is observed that the contours with relatively high magnitudes are distributed approximately at the left-top and right-bottom corner of the forced area. In the case with $\theta_1 = 30°$ and

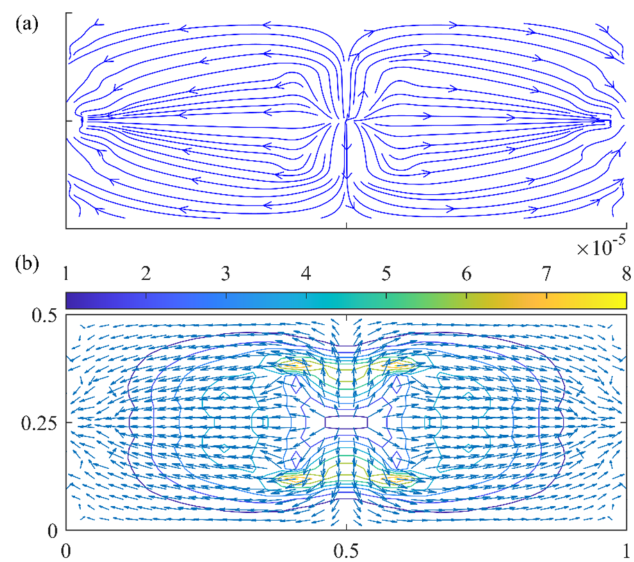

Fig. 16 Structural intensity in the laminated composite plate with $\theta_1 = 0°$ and $\theta_2 = 90°$ with area force excitation over the area of 0.25 m and 0.25 m at center point (0.5 m, 0.25 m) at a frequency of 1005.31 rad/s. **a** Streamline and **b** vector

$\theta_2 = 90°$, the fiber orientation in the 30° has large effects on the streamlines in the contacted area as shown in Fig. 15a. Large numbers of vectors from the source are pointing at the fiber angles in 30°. As a result, contours with relatively high magnitude occur at the right-top and left-bottom corner of the contacted area as Fig. 15b shown. The position of the vectors with relative high magnitudes around the interface between the forced and unforced areas is effectively shifted by changing the value of θ_1. A comparison between the Figs. 14 and 15 indicated that although the fiber angles at the contacted area are the same, the energy transmission at such position varies with designed fiber paths.

When the fiber angle θ_1 is decreased to 0°, large number of vectors are pointing from the source to the top and bottom edge of the plate first and then the directions of the vectors are altered from 90° to 0° slightly. It is clearly observed that the energy flows into the energy sink at the middle points of the left and right edge respectively. Figure 16b shows that the contours with high magnitudes are separately formed at the top and bottom edge of the forced area. Comparing Fig. 16 with the Fig. 7 that showing the structural intensity of the plate with $\theta_1 = \theta_2 = 0°$, the difference in the fiber angle from 0° to 90° in the forced area (i.e., θ_2) contributes to the formation of energy sink existing at the middle parts of left and right edges.

Vibration Energy Transmission on VAT Composite Plates with Curvilinear Fibers

The forced vibration behavior of the VAT plate with curvilinear fibers in $[\langle 0°, 90°\rangle]_4$ was examined and compared with that of conventional laminated composite plate in $\theta_1 = \theta_2 = 0°$, and the plate in $\theta_1 = 0°$ and $\theta_2 = 90°$ with straight fibers. The fiber orientation at every point is clearly defined by $\langle 0°, 90°\rangle$ and all layers of this four-layer plate are in the same configuration. Figure 16 shows the comparisons on the response amplitude of those three plates subjected to the area force over the area of 0.25 m and 0.25 m at the center point (0.5 m, 0.25 m). The peak value of the first resonance peak of the $[0°]_4$ composite plates at 216.63 rad/s is much larger than that of other plates. It is found that the first resonance frequency of the $[\langle 0°, 90°\rangle]_4$ plate with curvilinear fibers is 427.26 rad/s, which is much larger than that of other plates. Using curvilinear fiber paths, the first resonance peak is effectively shifted to higher frequency with lower peak value. The frequency range from the first peak to second peak is narrowed. With the increase in excitation frequency, the amplitude of the response of the composite plate with curvilinear fiber paths tends to decrease. Compared to the composite plate with straight fibers, the VAT plate performs at low-level vibration in a relative high-frequency range (Fig. 17).

Figures 18 and 19 show SI streamlines and vectors on the $\langle 0°, 90°\rangle$ laminated composite plates excited at its second and third excitation frequencies, 892.21 rad/s and 1275.49 rad/s. As the fiber angles from the beginning edge to the middle and then to the end edge slightly increased from 0° to 90° and then to 0°, the most energy from the center part flows to obvious energy sinks at the left-top and right-bottom corner of the plate, following the curvilinear fiber paths as the streamline shown in Fig. 18a. Compared to that the energy sink in Fig. 16a at the middle part of left and right edge, the positions of energy sinks are altered by curvilinear fibers and become more obvious. It is found that the streamlines around the energy sink become serried. The SI vector in Fig. 18b clearly shows the energy distribution on the plate, in which the contours with relatively high magnitudes are separately formed around the distorted middle line. As the excitation increased, the area of energy source is rotated and two recirculation regions are observed at the left-top edge and right-bottom edge as the Fig. 19a shown.

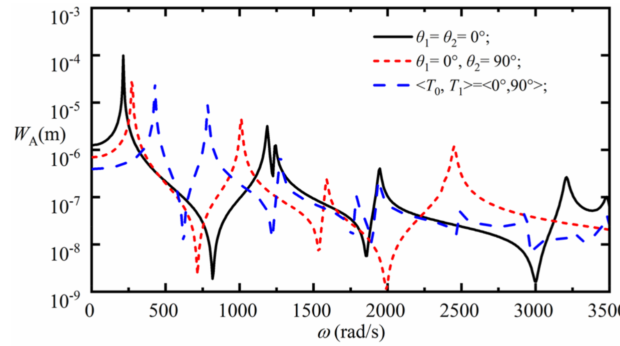

Fig. 17 The amplitude of the response (W_A) as a function of frequency at the center point (0.5 m, 0.25 m) on the laminated composite plate subjected to the area force over the area of 0.25 m and 0.25 m. Solid line: $\theta_1 = \theta_2 = 0°$; short dashed line: $\theta_1 = 0°, \theta_2 = 90°$; dashed space line: $\langle T_0, T_1\rangle = \langle 0°, 90°\rangle$

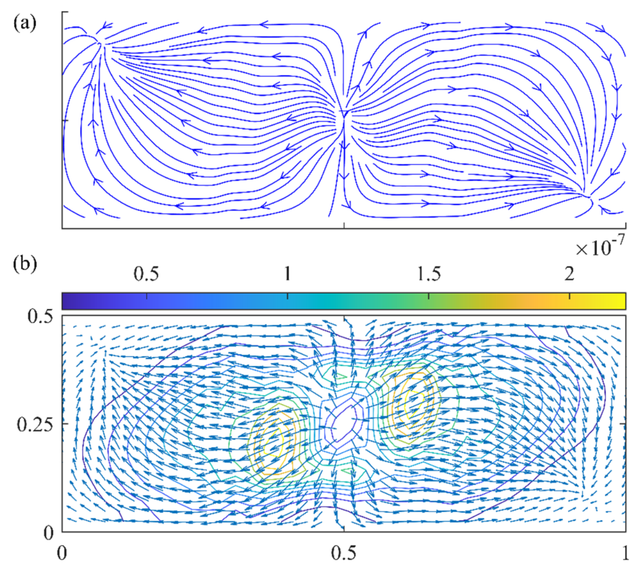

Fig. 18 Structural intensity in the laminated composite plate in $\langle T_0, T_1\rangle = \langle 0°, 90°\rangle$ with area force excitation over the area of 0.25 m and 0.25 m at center point (0.5 m, 0.25 m) at a frequency of 892.21 rad/s. **a** Streamline and **b** vector

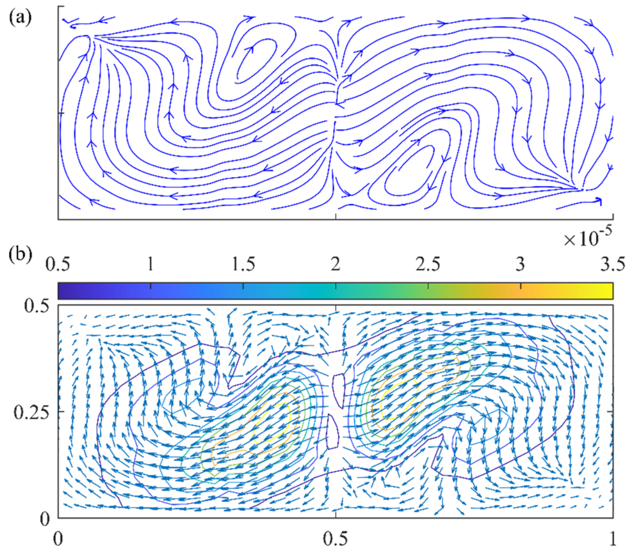

Fig. 19 Structural intensity in the laminated composite plate in $\langle T_0, T_1 \rangle = \langle 0°, 90° \rangle$ with area force excitation over the area of 0.25 m and 0.25 m at center point (0.5 m, 0.25 m) at a frequency of 1275.49 rad/s. **a** Streamline and **b** vector

Passing the complex vortex-type flow, some energy returns to the energy source but most energy is still transmitted into the energy sinks, formed at the left-top and right-bottom corner of the plate. Figure 19b shows that the contours of vectors with relatively high amplitudes around the central part are extended.

Conclusions

In this study, the forced vibration behavior of laminated composite plates with various fiber paths under distributed force excitations is investigated from the energy flow perspectives. The effects of the dimensions of plates and applied area force, as well as fiber paths on forced vibration behavior were studied. Structural intensity analysis was performed to determine energy transmission paths visually including streamline and vector representation of a variety of laminated composite plates.

The streamlines explicitly showed the energy transmission paths and vectors with contours clearly presented the distribution of vibration energy. The results showed that an increase in fiber angle in the forced area leads to the stiffness increasing in the lateral direction. This could effectively reduce the amplitudes of the first resonance peak. Increasing the fiber angle in the unforced area mainly leads to a narrower frequency range between the first and second peaks. Changing the angles of fibers around the edge can alter the position of energy sinks. The formation of vortex-type flows by designing fiber angles of forced area results in low-level vibration behavior. VAT provides enlarged design space for tailoring energy transmission paths of composite plates at some particular excited frequencies.

In summary, this study leads to new information on energy transmission between the forced and unforced areas of composite plates subjected to area force that can be used for enhanced vibration suppression by designing fiber angles. The power flow analysis or structural intensity analysis can be developed to clearly predict and evaluate the vibration energy flow behavior of complex composite structures subjected to various loading. The streamlines representations can be used to show clearly the vibration energy flow paths with excited structures.

Acknowledgements This work is supported by Zhejiang Provincial Natural Science Foundation of China under Grant number LQ23A020003 and LY22A020006, by the National Natural Science Foundation of China under Grant number 12172185, by the National Key Research and Development Program (2019YFA0706803), and by the Ningbo Municipal Natural Science Foundation Grant number 2022J174.

Author Contributions CZ: conceptualization, methodology, software, investigation, writing—original draft, data curation. GL: supervision, funding acquisition, project administration. SR: investigation, supervision. JY: conceptualization, investigation, supervision, writing—review and editing, funding acquisition.

Data availability The data supporting this study's findings are available from the corresponding author, upon reasonable request.

References

1. Reddy JN (2003) Mechanics of laminated composite plates and shells: theory and analysis, 2nd edn. CRC Press, Washington
2. Sayyad AS, Ghugal YM (2015) On the free vibration analysis of laminated composite and sandwich plates: a review of recent literature with some numerical results. Compos Struct 129:177–201
3. Thai HT, Choi DH (2013) A simple first order shear deformation theory for laminated composite plates. Compos Struct 106:754–763
4. Aagaah MR, Mahinfalah M, Jazar GN (2006) Natural frequencies of laminated composite plates using third order shear deformation theory. Compos Struct 72:273–279
5. Kan T, Swaminathan K (2001) Analytical solution for free vibration of laminated composite and sandwich plates based on a higher-order refined theory. Compos Struct 53:73–85
6. Grover N, Singh BN, Maiti DK (2013) Analytical and finite element modelling of laminated composite and sandwich plates: an assessment of a new shear deformation theory for free vibration response. Int J Mech Sci 67:89–99
7. Ribeiro P, Akhavan H, Teter A, Warminski J (2014) A review on the mechanical behaviour of curvilinear fiber composite laminated panels. J Compos Mater 48:2761–2777
8. Honda S, Narita Y (2012) Natural frequencies and vibration modes of laminated composite plates reinforced with arbitrary curvilinear fiber shape paths. J Sound Vib 331:180–191
9. Akhavan H, Ribeiro P (2011) Natural modes of vibration of variable stiffness composite laminates with curvilinear fibers. Compos Struct 93:3040–3047

10. Houmat A (2018) Three-dimensional free vibration analysis of variable stiffness laminated composite rectangular plates. Compos Struct 194:398–412
11. Abdalla MM, Setoodeh S, Güdal Z (2007) Design of variable stiffness composite panels for maximum fundamental frequency using lamination parameters. Compos Struct 81:283–291
12. Dobyns AL (1981) Analysis of simply-supported orthotropic plates subject to static and dynamic loads. AIAA J 19:642–650
13. Carvalho A, Soares CG (1996) Dynamic response of rectangular plates of composite materials subjected to impact loads. Compos Struct 34:55–63
14. Aslan Z, Karakuzu R, Okutan B (2003) The response of laminated composite plates under low-velocity impact loading. Compos Struct 59(1):119–127
15. Gliszczynski A, Kubiak T, Rozylo P, Jakubczak P, Bienias J (2019) The response of laminated composite plates and profiles under low-velocity impact load. Compos Struct 207:1–12
16. Lee SK, Kim MW, Park CJ, Chol MJ, Kim JM, Choi CH (2016) Effect of fiber orientation on acoustic and vibration response of a carbon fiber/epoxy composite plate: natural vibration mode and sound radiation. Int J Mech Sci 117:162–173
17. Noiseux D (1970) Measurement of power flow in uniform beams and plates. J Acoust Soc Am 47:238–247
18. Gavric L, Pavic G (1993) A finite element method for computation of structural intensity by the normal mode approach. J Sound Vib 164:29–43
19. Li YJ, Lai JCS (2000) Prediction of surface mobility of a finite plate with uniform force excitation by structural intensity. Appl Acoust 60:371–383
20. Xu XD, Lee HP, Lu C, Guo JY (2005) Streamline representation for structural intensity fields. J Sound Vib 280:449–454
21. Khun MS, Lee HP, Lim SP (2004) Structural intensity in plates with multiple discrete and distributed spring-dashpot systems. J Sound Vib 276:627–648
22. Xu XD, Lee HP, Wang YY, Lu C (2004) The energy flow analysis in stiffened plates of marine structures. Thin-Walled Struct 42:979–994
23. Xu XD, Lee HP, Lu C (2004) The structural intensities of composite plates with a hole. Compos Struct 65:493–498
24. Liu ZS, Lee HP, Lu C (2005) Structural intensity study of plates under low-velocity impact. Int J Impact Eng 31:957–975
25. Liu ZS, Lee HP, Lu C (2006) Passive and active interior noise control of box structure using structural intensity method. Appl Acoust 67(2):112–134
26. Cho DS, Choi TM, Kim JH (2016) Structural intensity analysis of stepped thickness rectangular plates utilizing the finite element method. Thin-Walled Struct 109:1–12
27. Chen T, Liu LM, Liu QN, Song FX, Feng ZW (2021) Influences of the temperature rise on the vibration energy flow in a dissipative elastic metamaterial plate based on the structural intensity approach. Thin-Walled Struct 160:107347
28. Wang LG, Chen T (2019) Structural intensity analysis of the cantilevered plate under thermal load. Thin-Walled Struct 139:209–218
29. Mahapatra K, Panigrahi SK (2020) Dynamic response and vibration power flow analysis of rectangular isotropic plate using fourier series approximation and mobility approach. J Vib Eng Technol 8:105–119
30. Farag H, Pan J (1998) On the free and forced vibration of single and coupled rectangular plates. J Acoust Soc Am Am 104:204–216
31. Cuschieri JM, McCollum MD (1996) In-plane and out-of-plane waves power transmission through L-plate junction using the mobility power flow approach. J Acoust Soc Am 100(2):857–870
32. Kessissoglou NJ (2004) Power transmission in L-shaped plates including flexural and in-plane vibration. J Acoust Soc Am 115(3):1157–1169
33. Wang ZH, Xing JT, Price WG (2002) An investigation of power flow characteristics of L-shaped plates adopting a substructure approach. J Sound Vib 250(4):627–648
34. Wu WW, Yin XW, Li H, Zhong KK (2017) Power flow analysis of built-up plate structures using the dynamic stiffness method. J Vib Control 24:1–7
35. Chen YH, Jin GY, Zhu MG, Liu ZG, Du JT, Li WL (2012) Vibration behaviours of a box-type structure built up by plates and energy transmission through the structure. J Sound Vib 331(4):849–867
36. Petrone G, Vendittis MD, Rosa SD, Franco F (2016) Numerical and experimental investigations on structural intensity in plates. Compos Struct 140:94–105
37. Capasso PJ, Petrone G, Kleinfeller N, Rosa SD, Adams C (2021) Modeling of fiber composite structures for the calculation of the structural intensity. Compos Struct 262:113631
38. Zhu CD, Yang J, Rudd C (2021) Vibration transmission and power flow of laminated composite plates with inerter-based suppression configurations. Int J Mech Sci 190:106012
39. Zhu CD, Yang J, Rudd C (2021) Vibration transmission and energy flow analysis of L-shaped laminated composite structure based on a substructure method. Thin-Walled Struct 169:108375
40. Zhu CD, Li G, Ruan SL, Yang J (2022) Vibration suppression and energy flow tailoring of coupled metal and composite plates with curvilinear fibers. Mech Adv Mater Struct. https://doi.org/10.1080/15376494.2022.2141385
41. Zhu CD, Yang J (2022) Vibration transmission and energy flow analysis of variable stiffness laminated composite plates. Thin-Walled Struct 180:109927
42. Zhu CD, Li G, Yang J (2023) Vibration analysis of laminated composite panels with various fiber angles. In: Dimitrovová Z, Biswas P, Gonçalves R, Silva T (eds) Recent trends in wave mechanics and vibrations. WMVC 2022. Mechanisms and machine science, vol 125. Springer, Cham. https://doi.org/10.1007/978-3-031-15758-5_98
43. Xing JT, Price WG (1999) A power-flow analysis based on continuum dynamics. Proc R Soc Lond A 455:401–436